metals

MDPI

Article

Modification of the Cu/W Interface Cohesion by Segregation

Rishi Bodlos [1], Daniel Scheiber [1], Jürgen Spitaler [1] and Lorenz Romaner [1,2,*]

[1] Materials Center Leoben Forschung GmbH (MCL), Roseggerstraße 12, A-8700 Leoben, Austria
[2] Department of Materials Science, Montanuniversität Leoben, Franz-Josef Straße 18, A-8700 Leoben, Austria
* Correspondence: lorenz.romaner@unileoben.ac.at

Abstract: Cu/W composites are widely used in various industrial fields as they show thermomechanical properties suitable for a wide range of applications. Additionally, in semiconductor products, WTi in contact with Cu acts as a barrier material between Cu and Si/SiO_2. Therefore, the bonding behavior of both Cu/W and Cu/WTi is of great economical interest, also with respect to the effects that impurities could have on the behaviour of the Cu/W(Ti) interface. The segregation behavior of relevant impurities has not been studied in detail before. In this work, we create atomistic models of the Cu/W and Cu/WTi interfaces, compare their energetics to previously known interfaces and study the effect of segregation on the interface cohesion. We find that all investigated segregants, i.e. Ti, Cl, S, Al, H, O, and vacancies weaken the cohesion of the interface.

Keywords: segregation; density functional theory; interfaces

check for updates

Citation: Bodlos, R.; Scheiber, D.; Spitaler, J.; Romaner, L. Modification of the Cu/W Interface Cohesion by Segregation. *Metals* **2023**, *13*, 346. https://doi.org/10.3390/met13020346

Academic Editors: Pavel Lejček and Miroslav Černý

Received: 27 November 2022
Revised: 15 January 2023
Accepted: 26 January 2023
Published: 9 February 2023

Copyright: © 2023 by the authors. Licensee MDPI, Basel, Switzerland. This article is an open access article distributed under the terms and conditions of the Creative Commons Attribution (CC BY) license (https://creativecommons.org/licenses/by/4.0/).

1. Introduction

Cu/W composites are interesting materials used in numerous applications such as contact materials, heat sinks, electrodes and vacuum interrupters [1,2]. Their physical properties including thermal conductivity, thermal resistance and mechanical properties are in between those of Cu and W and can be fine-tuned by varying alloy composition and grain size [3]. The reason why CuW forms a composite or a pseudoalloy is that copper and tungsten are mutually immiscible in their solid state [4,5] and form a 2-phase system [1,2,6]. In addition to a pseudoalloy, Cu/W can also be created as a layered metal system where Cu and W phases are sputtered in thin layers on top of each other creating interfaces in between. These Cu/W layered systems show promising characteristics for electrical, mechanical and thermal application with common applications being reactor facing materials, heat sinks and electrical contacts [7]. As thickness is in the nm range, interfaces and grain boundaries take up a significant portion of the overall volume and have a large influence on the properties of the layered metal system. For Cu/W pseudoalloys and layered systems, there exist publications on mechanical, chemical, elastic, thermal, interfacial and segregation properties [4,7–11].

Cu/W and in particular Cu/WTi layered systems are commonly found in semiconductor devices. Here, WTi is typically used as a diffusion barrier to prevent migration of Cu to Si and SiO_2 components which could lead to the formation of copper silicides. These in turn are known to reduce the performance and can lead to failure of the device [12,13]. W or Ti alone were observed to be chemically stable only up to 400 °C for 1 h after which a reaction with Cu or Si occurred. In contrast, WTi prevents Cu diffusion to Si up to temperatures above 600 °C for 4 h with barrier failure observed at 700–800 °C. Additionally slight Ti diffusion from WTi to the silicon at 400 °C and above was observed, which leads to an improvement in adhesion to the silicon layer and prevention of harmful WSi_3 at 600 °C and below [14]. Therefore, the mechanical and chemical properties of Cu/WTi interfaces are of great relevance.

As the crystal structure of Cu is fcc and that of W is bcc, they form a heterophase boundary. Regarding the preferential orientation relation of fcc and bcc for Cu/W, a [111]

and a [110] texture were found for Cu and W in XRD experiments, respectively [10,15–17]. In previous theoretical works carried out on a similar fcc-bcc system, i.e., Cu/Nb, such textures have been found to lead to Kurdjumov Sachs (KS) and Nishiyama Wassermann (NW) interfaces and variations thereof [18–23].

At the nanoscale of Cu/W and Cu/WTi layered metal systems, interface properties such as interface energy (γ) and work of separation (W_{sep}) become crucial [6]. The bonding strength of interface and grain boundaries can be influenced by alloying elements or impurities that exhibit a strengthening or weakening effect on the cohesion. Hence, the behavior of additives, especially in terms of segregation, is crucial to the understanding of bonding behaviour [24]. However, an exact quantification of segregation elements and their effects on bonding strength in solids can be difficult when using experimental methods, as individual methods have resolution limits and requirements that make them only suited for certain situations. Auger electron microscopy for example requires a brittle interface and therefore elements that strengthen or have no effect on the cohesion cannot be measured by this method [25]. Additionally, sample preparation such as crack opening can introduce new defects that are then falsely attributed to segregation [25]. Therefore, atomistic simulation such as DFT can be useful to understand the segregation tendencies and mechanism of strengthening or weakening of cohesion based on chemical composition. In the literature, segregation in Cu or W has mostly focused on grain boundaries and surfaces and has been studied extensively by various authors [26–31].

The results of Scheiber et al. [29] show segregation profiles for a wide range of elements all of which segregate from the W bulk to either the surface or the grain boundary. The strongest segregants to the surface are F, Cl, Na, S and O; all highly reactive elements that, either directly or in combination with O, form W compounds. B, C, Ni and Co are the strongest GB segregants in W; however, all of them also form intermetallic compounds and alloys with W. Zhang et al. [30] reported a GB segregation energy of -0.57 eV for Re to the W $\Sigma5(310)[001]$ GB. Combined with the low repulsion of Re-Re, this led to the formation of planar Re structures at increased Re concentration. Overall, a strengthening of the grain boundary was observed. Other smaller elements that segregate to the W GB such as H, He, Be and Li were found to decrease the GB cohesion and instead cause an embrittling effect [31–33]. Experimental confirmation is, however, difficult as microstructural effects have a much larger influence on bonding strength than impurities and therefore can mask them [34].

Razumovskiy et al. calculated segregation energies of Ag, Au, Se, Ge, Ni, Co, and Bi in Cu GBs and compared them with experimental measurements. Aside from Ni and Co, the other elements showed a strong segregation behaviour to the free surface and would therefore lead to a decohesion of Cu. Ni and Co exhibited anti-segregation [35]. Hono et al. measured segregation in Cu with atom probe microscopy and discovered oxidation of copper at the surface and enrichment of O at the GB [36]. Nieh et al. also observed an O enrichment at the Cu GB via Auger electron spectroscopy resulting in an embrittlement of the material [37].

In addition to these calculations of grain boundary and surface segregation, the segregation of H, He and Zr in Cu/W interfaces has also been studied with coherent cells [7,38,39]. As these cells are very small and coherent, the misfit strain is very high. Therefore, their interface energetics can differ significantly from incoherent cells. This can also have an effect on the segregation energy. Hydrogen was shown to weaken the cohesion of the Cu/W interface in an interstitial position while slightly increasing cohesion when being 1–2 layers above the interface. Zr was predicted to have a strengthening effect on the Cu/W interface; however, these predictions appear highly questionable. Although no segregation data for the Cu/WTi system could be found, Ti segregation in WTi has been studied by Schuh et al. predicting a decomposition of WTi at higher temperature and Ti concentration as observed by experiments [40]. The exact mechanism of this decomposition, however, is disputed as it contradicts recent findings [29,41,42].

For Cu/WTi and WTi, nearly no segregation data are available and, in addition, for Cu and Cu/W, several segregants such as Cl, S and O have not been calculated yet, despite Cl and S being major corroding agents for both W and Cu. In addition, O is known to bind strongly to W and Cu interfaces.

In this work, we provide a detailed study on the interface energetics and segregation of a variety of solutes at the Cu/W and Cu/WTi interface. We first extend the results of our previous work [43] with respect to the pure (unsegregated) interfaces. Then, we elucidate the preferential occupation of interfacial sites by the different solutes and discuss their effect on the work of separation which provides rational guidelines for the design of Cu/W and Cu/WTi-based heterostructures.

2. Methodology

2.1. Interfaces

For the orientation relationships, we chose four different interfaces, which can be seen in Figure 1. The structure of the KS and NW interface have been discussed in our previous work [43]. For these two interface types, which occur most frequently in nature, the closed packed planes of the respective crystal structures, i.e., the [111] plane for Cu and the [110] plane for W, are coplanar and meet at the interface. The KS2 and NW2 interface models are based on the KS and NW orientation relation with the same three pairs of planes being parallel. However, the Cu[112]//W[112] planes form the interface for KS2 and the Cu[110]//W[001] planes for NW2. KS2 and NW2 are often seen in roll bonded multi layers as these interfaces have been shown to be stable under plastic deformation [22,23].

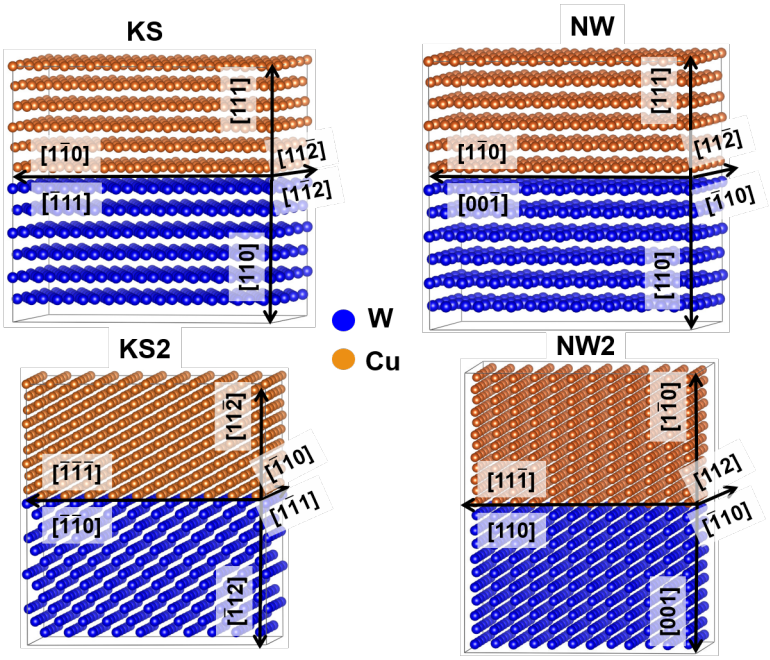


Figure 1. The four interfaces examined: KS, NW, KS2 and NW2. KS2 and NW2 are variations of NW and KS.

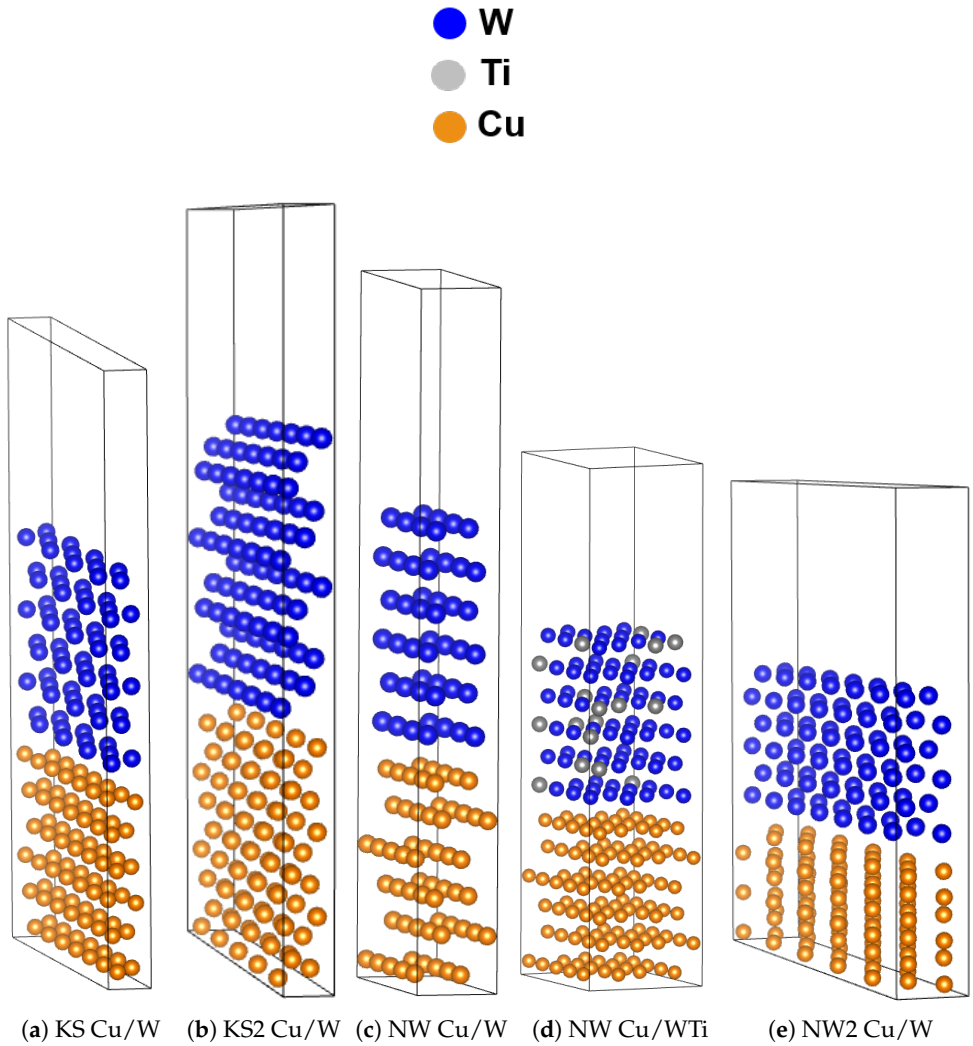
2.2. Atomistic Models

The number of Cu, W and Ti atoms and cell dimensions used for the Cu/W and Cu/WTi interfaces can be seen in Table 1 and the cells in Figure 2. The setup of the cell including layer thickness, vacuum and optimized lattice parameters is identical to that of our previous work [43]. To simulate a WTi solid solution, a supercell with minimized Warren–Cowley short range order parameter was generated [44–46]. The concentration of WTi that was used for the cell in this work is 18.75 percent Ti. This concentration was shown to have the lowest formation energy and volume in our previous publication [42]. The interface model chosen for Cu/WTi corresponds to the NW orientation relationship

according to the results of Section 3.1. In order to simulate segregants in bulk Cu, we used a 108 atom Cu cell with the equilibrium lattice parameter of Cu and no vacuum. For bulk W, we used a 128 atom cell again without vacuum and with the equilibrium lattice constant. The Cu grain boundary (GB) calculations were conducted using the same cell as in Razumovskiy et al. [35].

Table 1. Number of atoms in each interface cell and cell dimensions (Å).

Interface Model	Cu Atoms	W Atoms	Ti Atoms	l (X)	l (Y)	l (Z)
NW	60	48	0	12.77	4.49	38.61
NW WTi	120	78	18	12.76	8.97	38.59
KS	84	72	0	2.70	31.15	38.61
NW2	90	84	0	31.52	4.49	29.77
KS2	90	84	0	31.52	2.70	41.46



(**a**) KS Cu/W (**b**) KS2 Cu/W (**c**) NW Cu/W (**d**) NW Cu/WTi (**e**) NW2 Cu/W

Figure 2. Cells used for interface calculations. Cu/W energetics were calculated for the KS, KS2, NW and NW2 cells, while Cu/WTi energetics were calculated for the NW cell only. For an explanation of the used abbreviations please see the text.

2.3. Calculation Parameters

Our calculations were carried out using the Vienna Ab-Initio Simulation Package (VASP) under periodic boundary conditions using the PBE functional [47] and the projector

augmented wave method. To determine the number of k-points, the product of length of the cell and number of k-points in the x- or y-direction was chosen to be as close as possible to 35 k-points $\times$ Å to ensure a converged k-point sampling for all unit cells of different dimensions. Just 1 k-point is used in the perpendicular z direction. The cut-off energy was chosen to be 300 eV, ionic relaxations were conducted using the conjugate gradient algorithm. Cu was calculated using 11 valence electrons ($3d^{10}4s^1$), while W and Ti were calculated using 12 ($5p^6 5d^4 6s^2$) and 10 valence electrons ($3p^6 3d^2 4s^2$), respectively. As with the NW and KS interfaces taken from our previous work, the KS2 and NW2 interfaces were optimized using the stress balancing method [48].

2.4. Interface Energetics

The work of separation (W_{sep}), which is the energy needed to completely separate the W and Cu slab, is calculated via the following equation:

$$W_{sep} = \frac{(E_{Cu} + E_{W(Ti)}) - E_{Cu/W(Ti)}}{A}. \tag{1}$$

where E_{Cu}, $E_{W(Ti)}$ and $E_{Cu/W(Ti)}$ are the energies of the Cu, W(Ti) and Cu/W(Ti) slab, respectively, with W(Ti) denoting both W and WTi. In this calculation, the cell dimensions of the Cu, W(Ti) and Cu/W(Ti) cells in x-, y- and z-directions are set to the same value, see Table 1.

The interface energy is the energy required to form an interface in the perfect bulk material and is defined as:

$$\gamma = \frac{E_{Cu/W(Ti)} - \frac{E'_{Cu} + E'_{W(Ti)}}{2}}{A}. \tag{2}$$

In this case, E'_{Cu} and $E'_{W(Ti)}$ are the energies of the isolated Cu and W(Ti) slab, respectively, where the amount of layers has been doubled compared to the ones in the interface cell.

The segregation energy is the energy needed for an atom to move from a reference structure (e.g., the Cu or W bulk) to a defect position such as the grain boundary or the interface. To allow us to compare results between different simulation cells such as the Cu GB, W GB and segregation to different positions within Cu/W and Cu/WTi, we need to establish a universal reference, which in this work is bulk Cu, as the much thicker Cu layer, in contrast to the sputtered W(Ti), is usually deposited via CVD from a solution containing various additives and hence is the source of impurities in Cu/W(Ti). For calculations at the Cu GB, we use the following formula:

$$E_{seg} = (E^X_{Cu_{GB}} - E_{Cu_{GB}}) - (E^X_{Cu_B} - E_{Cu_B} \pm \mu_{\mathrm{M}}); (M = Cu). \tag{3a}$$

$$\mu_{\mathrm{M}} = \frac{E_{M_B}}{n_{M_B}}. \tag{3b}$$

Here, X denotes the segregant (i.e., the segregating element), $E^X_{Cu_{GB}}$ is the energy of the Cu GB slab including the segregant, $E_{Cu_{GB}}$ the energy of the Cu GB slab without segregant, $E^X_{Cu_B}$ the energy of the bulk Cu slab including the segregant and E_{Cu_B} the energy of the bulk Cu slab without segregant, respectively. μ is the correction term to account for segregation where the atom switches from substitutional to interstitial position or vice versa, thereby adding or subtracting an atom. If there is no such transition, μ is 0. Here, n_{M_B} corresponds to the number of atoms in the bulk cells used to calculate E_{M_B}.

For segregation of X to the W GB, literature data are available where an analogous equation to (3a) has been used. Since here the reference for all segregation energies is the Cu bulk, the literature segregation energies E'^{X}_{seg} are shifted by a constant B:

$$E_{seg} = E'^{X}_{seg} + B \tag{4a}$$

$$B = (E^{X}_{W_B} - E_{W_B} + \mu_{\mathrm{W}} z) - (E^{X}_{Cu_B} - E_{Cu_B} + \mu_{\mathrm{Cu}} z) \tag{4b}$$

$$\mu_{\mathrm{M}} = \frac{E_{M_B}}{n_{M_B}}; (M = Cu, W). \tag{4c}$$

B accounts for segregation from bulk Cu to bulk W. Here, z is the number of atoms that get displaced by the segregant and is 0 in case of interstitial segregation and 1 in case of substitutional segregation.

For Cu/W and Cu/WTi, the segregation energy is calculated as:

$$E_{seg} = (E^{X}_{Cu/W(Ti)} - E_{Cu/W(Ti)}) - (E^{X}_{Cu_B} - E_{Cu_B} + C \pm \mu_{\mathrm{M}}); (M = Cu, W, Ti). \tag{5a}$$

$$C = \mu_{\mathrm{M}} - \frac{E_{Cu_B}}{n_{Cu_B}}. \tag{5b}$$

Here, $E^{X}_{Cu/WTi}$ and $E_{Cu/WTi}$ are the energies of the Cu/WTi supercells with and without segregant. While the reference is bulk Cu, segregation in Cu/WTi can occur on both the Cu and WTi side of Cu/WTi. C accounts for the change of the number of Cu and W or Ti atoms during segregation on the WTi side. If segregation takes place at the Cu part of the Cu/WTi system, C becomes 0.

For Cu/W and Cu/WTi, the strength of embrittlement (S_{Emb}) is of particular interest as it shows us the change in interfacial strength as the chemistry changes. A positive S_{Emb} denotes improved cohesion while a negative S_{Emb} denotes an embrittlement of the interface. In essence, it can be calculated as the difference in segregation energy between the interface and surface. As many terms cancel in this difference, the quantity is given simply by:

$$S_{Emb} = E^{X(surf)}_{Cu/WTi} - E^{X(int)}_{Cu/W(Ti)} \tag{6}$$

with $E^{X(surf)}_{Cu/WTi}$ and $E^{X(int)}_{Cu/WTi}$ denoting the energy of the Cu/WTi supercell with segregant X at the surface and the interface position, respectively.

3. Results and Discussion

3.1. Interface Energy and Work of Separation

In our previous work, we had focused on the interface energetics and structural relaxation of KS and NW interfaces in Cu/W and Cu/Nb [43]. As a first step in the current work, the interface energetics of the KS2 and NW2 interface models, which are closely related to the KS and NW interface models, were calculated to compare and contrast. The comparison of the calculated interface energy and work of separation for the four interface models is presented in Figure 3. NW and KS exhibit a lower interface energy as KS2 and NW2 indicating increased structural stability; however, in terms of W_{sep}, the NW2 interface is shown to be the most stable. A similar effect has been observed for Cu/Nb by Demkowicz et al. [49]. In addition to the increased W_{sep}, both Cu/Nb KS2 and NW2 were shown to have additional advantages over KS and NW interfaces such as higher shear resistance, higher retention of hardness after annealing and the ability to absorb point defects [23,50,51]. Whether these properties are also present in NW2 Cu/W is currently unclear, however, as the shear resistance and thermal stability of Cu/Nb KS2 are attributed to its jagged interface [23,50,51], the same can be assumed for KS2 Cu/W. The interface energy γ is lowest for the NW interface, which was therefore chosen for the Cu/WTi

interface and for segregation calculations. It matches well with XRD measurements of Cu/W that show a clear Cu(110) and W(111) texture as it is the case with KS and NW interfaces [15,16]. The interface energies and W_{sep} of Liang et al. [52] and Wang et al. [53] partially match our calculations, with the coherent cells using the Cu lattice constant being in close agreement with our results. The results that do not match ours well use a coherent cell and the W lattice constant. These contrasting results for coherent cells have also been observed and discussed in our previous work. For studying the influence of Ti in WTi on the energetics of the Cu/WTi interface, we replaced the W slab with a so-called Special Quasirandom Structure (SQS) of W-18.75%Ti; see Figure 2 in the NW orientation. As seen in Figure 3, this results in a decrease in both γ and W_{sep}. Overall, however, the results of Cu/W and Cu/WTi are relatively close to each other.

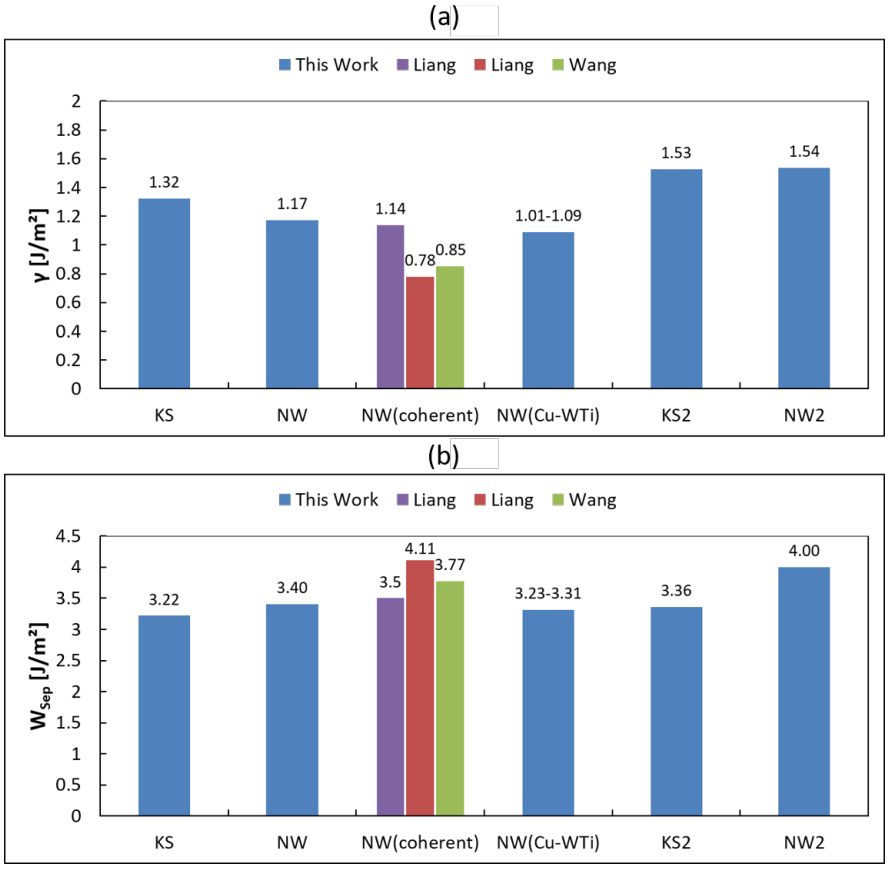


Figure 3. The interface energy γ (**a**) and the work of separation W_{sep} (**b**) of the four interfaces. The results are also compared with the ones by Liang et al. [52] and Wang et al. [53].

3.2. Segregation of Elements

3.2.1. GB Segregation

The sites considered for GB segregation in Cu can be seen in Figure 4. These sites and the overall methodology are analogous to the approach in Razumovskiy et al. [35] and Scheiber et al. (using Equation (3b)) [29].

As seen in Figure 5, all elements except Al segregate to the Cu GB. Substitutional positions are preferred for Cl and S while O and H prefer the interstitial position. Other segregation states such as Cl (interstitial site to interstitial site) or H (substitutional site to substitutional site) are not considered, as these correspond to a higher energetic bulk starting position. The segregation energy of Al is 0.01 eV, which corresponds to anti-segregation; however, the energy is so low that it is negligible in view of other minor factors that can influence the energy, such as artifacts of the Cu surface or the GB. To further analyse the implications of a segregation to the GB, an analysis of these energies with

segregation energies to the Cu and W surfaces, the W GB and the Cu/WTi interface is performed in the following sections.

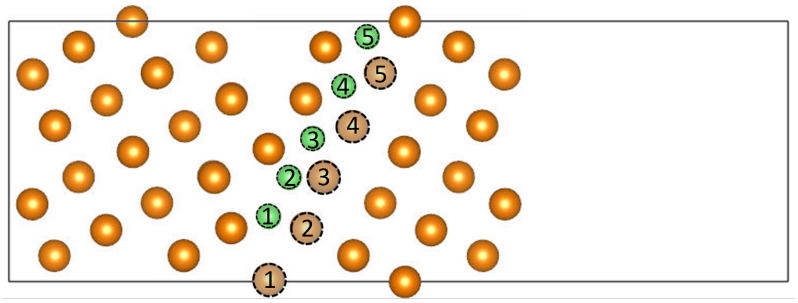


Figure 4. A schematic representation of the $\Sigma 5(210)[100]$ tilt CSL GB in fcc Cu. Numbers denote investigated lattice sites for solute segregation. Interstitial sites are marked in green.

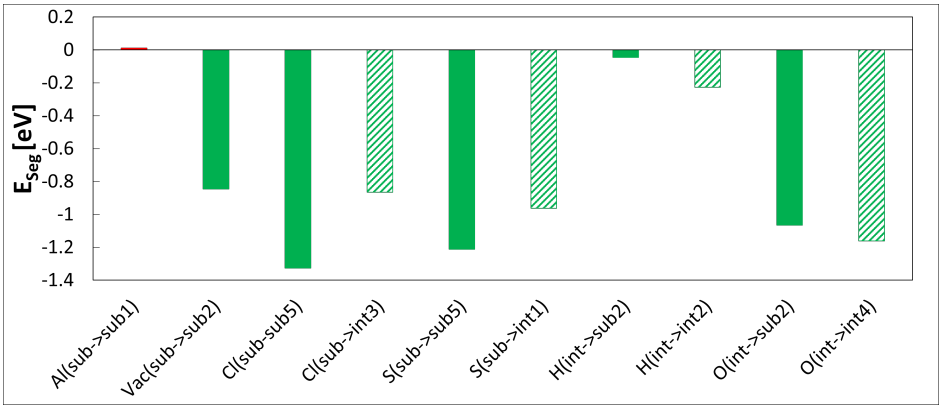


Figure 5. Segregation energies of Al, S, Cl, H, O and vacancies at Cu GB. The substitutional position is shortened to sub and the interstitial to int, with the number indicating the position on Figure 4. Segregation to the interstitial site is marked with diagonal stripes while segregation to substitutional site is filled.

3.2.2. Segregation at the Cu/W Interface

In Figure 6, we show the segregation profile of a number of elements to various positions at the NW Cu/W interface (see Figure 2c) with reference state in the Cu bulk (using Equation (4c)). By definition, W atoms show no change in segregation energy when moving inside the W slab. At the Cu side of the Cu/W interface, the segregation energy of W increases, reaching a maximum at the Cu surface, while the energy at the interface is halfway between the one inside the W and Cu slab. Cu segregation shows nearly the opposite behaviour, with segregation in W being unfavorable and segregation energy equal to zero (by definition) in Cu. Ti segregation is most favorable at the W surface and then gets slightly less favorable till the W side of the Cu/W interface. The overall change in energy in W is low, however, which could be due to the high stability of WTi at low Ti concentrations [41,42]. In Cu, the segregation energy for Ti increases, with the maximum at the Cu surface. This reflects the fact that no mixing of the phases takes place, e.g., Ti and W do not enrich in Cu or vice versa which reflects the stability of WTi as a diffusion barrier.

While segregation energy of aluminium is higher in most positions of W than in Cu, the W surface is the position that shows the strongest segregation tendency. For S and Cl, segregation in W is also unfavourable with the W surface, nevertheless being the lowest in energy followed by the Cu surface and the interface. Vacancies show a slight preference for the Cu surface and the Cu/W interface compared to the Cu bulk while segregation to W bulk is unfavourable.

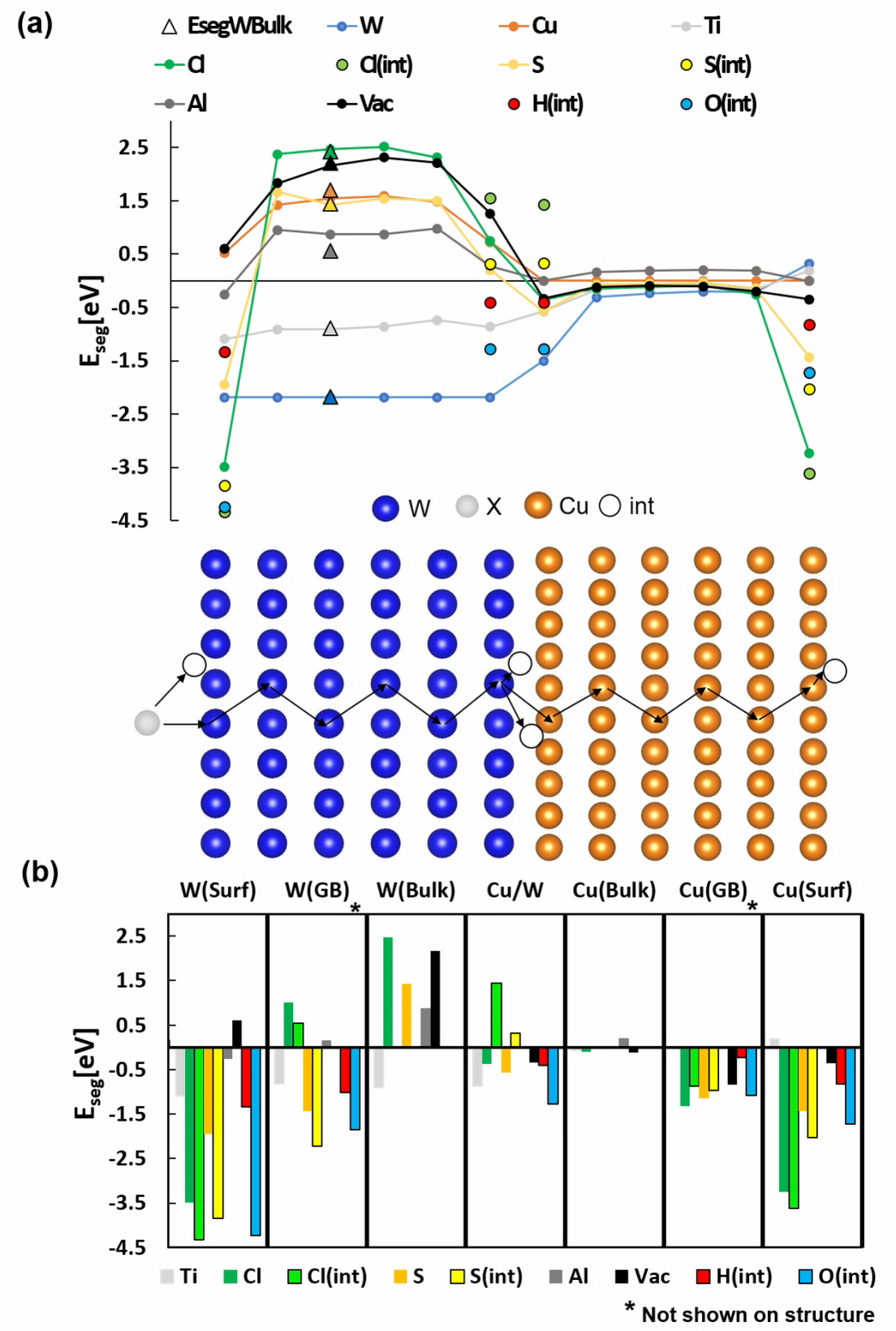


Figure 6. Segregation profile of Ti, Cl, S, Al, H, O and vacancies in Cu/W. (**a**) shows the segregation along the cell with Cu_{Bulk} as reference. The triangles show the segregation energy with respect to W_{Bulk}; (**b**) shows the segregation energy for selected positions, with the data for W_{GB} taken from Ref. [29]. The lowest energy site is shown for Cu/W, the Cu GB and the W GB.

Comparing the bulk positions in the Cu and W (triangle) reference with the same positions in the Cu/W cell, we can only see minor shifts in energy. Therefore, it can be concluded that the segregants do neither react significantly to the strain of the cell nor to the change in packing density between the bulk cell and the interface cell. Looking at the interstitial elements, namely Cl, S, H and O, we can see that surfaces are preferred over the interface position. The Cu matrix only leads to weak segregation tendencies for H and O while the W surface yields a higher segregation tendency for both elements. In Figure 7, we can see the positions the elements occupy after segregation with the adatom position being preferred over an interstitial site. Figure 6b) includes the grain boundary segregation energies for the Cu GB and that of the W GB, the latter of which were converted from [29] by shifting the reference to bulk Cu. The overall trend between W surface and GB matches that are calculated by Scheiber et al. with a minor shift in absolute values due to differences in chosen surface and exchange–correlation potential [29]. By looking at this chart and summarizing the previous points, we can conclude that, while the interface seems more favourable than the Cu bulk, it was not the most preferred site for any of the investigated elements. Instead, the surfaces were the preferred site for segregation followed by the grain boundaries.

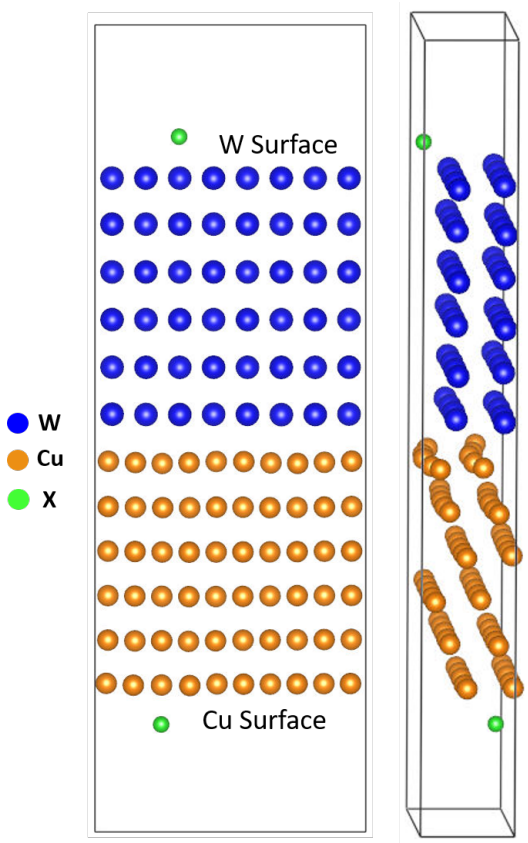


Figure 7. Positions considered for surface segregation of Cl, S, H and O (green atom).

3.2.3. Interface Positions

Figure 8 shows the segregation energies for different substitutional positions in the interface plane. This is analysed for both Cu and W side of the interface for Ti, while Cl and S were only tested at the Cu side. The overall difference for the positions is minor. The largest variations are seen for S that has a slight fluctuation, but on level that is low in magnitude compared to the overall segregation energy, i.e., the average value for S segregation is −0.62 eV, while maximal and minimal values are −0.66 eV and −0.57 eV, respectively. This confirms our conclusions from our previous publication [43] where the

γ-surface and relaxation of NW Cu/W interface revealed that the positions within the Cu/W interface were very close in energy and therefore nearly equivalent.

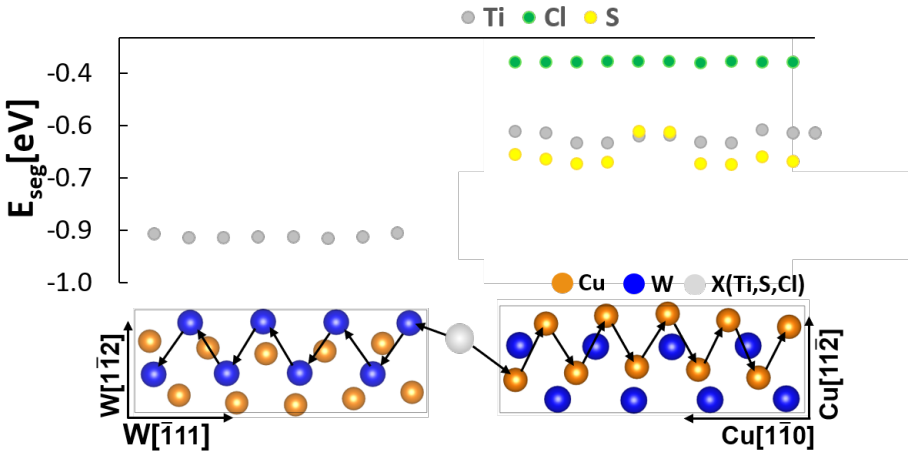


Figure 8. Energy of Ti, Cl and S as a function of position along the Cu[111]//W[110] interface. The image shows a top view of the interface layers from both the W(left) and the Cu(right) side. Cl and S were only tested at the Cu interface.

3.3. Cohesion

Figure 9 shows the strength of embrittlement (using Equation (6)) of the investigated elements in Cu/W. All of the segregants result in a weakening of the Cu/W interface due to their stronger segregation tendencies to the Cu and W surfaces than to the interface. The only strengthening solute is Ti at the Cu side of the interface, a position that is unfavourable for Ti compared to the W side and hence unlikely to be occupied except as an intermediary of a possible CuTi intermetallic phase. The effect of H on cohesion of Cu/W is similar to but slightly stronger than that observed by Ma et al. [7]. However, simulation cell, computational parameters, interface model and exchange–correlation potential differ. O, S and Cl are the strongest surface segregants and therefore show the largest effect. In fact, in Ref. [54], we calculated the cohesion of a Cu/W slab containing an entire mono-layer containing 8 O atoms, which showed a decrease in Cu/W interface cohesion by a factor of four times compared to that of a single O atom. Cl and S are also well known corrosive agents for Cu and are therefore avoided in general. Additionally, we compared our results on the influence of Zr segregation on the cohesion of the Cu/W interface with the results of Wang et al. [38]. This comparison is discussed in more detail in the Appendix A.

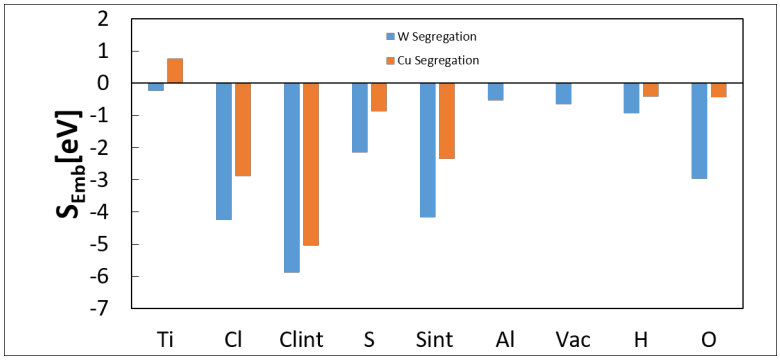


Figure 9. Strength of embrittlement with the segregating element at the Cu (orange) and W (blue) interface site for the NW Cu/W interface.

3.4. Cu/WTi Segregation and Cohesion

As Cl shows the largest effect on interface cohesion and is therefore of prime interest, it is taken as an exemplary element for studying the Cu/W(Ti) interface. The results on segregation (using Equation (3b)) are presented in Figure 10. To take effects of the local chemical environment into account, we chose two different paths through the W(Ti) slab with a different average number of surrounding Ti atoms. For Cl, it seems to be energetically favorable to have a large number of surrounding Ti atoms. However, this observation was made at all positions with the overall trend of the segregation profile not changing. This means that an increased concentration of titanium near or at the interface causes the same stabilisation of Cl as Ti at or near the surface, which results in a negligible change in strength of embrittlement compared to the overall energy, namely −4.24 eV for Cu/W and −3.72 eV and −4.06 eV for path 1 and 2 in Cu/WTi, respectively. The larger difference in path 1 from the strength of embrittlement of Cu/W compared to path 2 is mostly due to the higher concentration of Ti close to the interface compared to the surface in path 1, thereby strengthening the interface and increasing the cohesion. A WTi solid solution on the other hand is assumed to have the same Ti concentration across the entire material on average, especially since the segregation tendencies of Ti in W are very low as previously shown in Figure 6. Hence, the difference in strength of embrittlement of Cu/W and Cu/WTi can be assumed to be even lower than what path 1 and 2 predict.

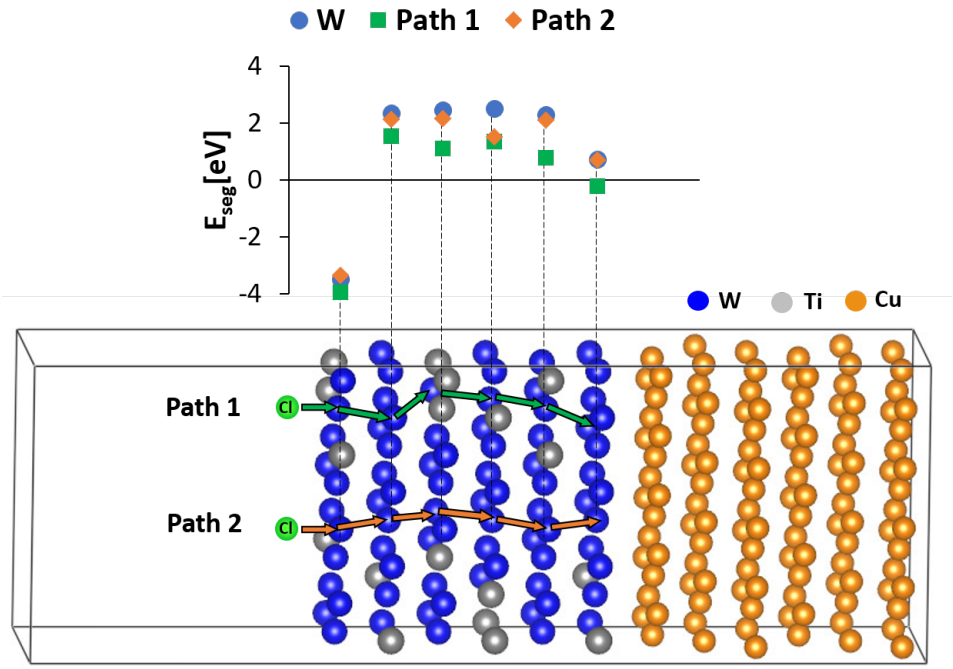


Figure 10. Segregation profile of Cl in NW Cu/WTi at different positions to simulate different local Ti concentrations as well as comparison to pure Cu/W interface.

4. Conclusions

In this work, we calculated the segregation of various elements to the Cu/W interface and the effect of segregation on the cohesion properties. To identify a relevant interface for the segregation calculations, we calculated the interface energy of four different Cu/W interfaces, two of which, KS and NW, have already been discussed in our previous work [43]. In comparison to the well-known KS and NW interfaces, we find that the KS2 and NW2 interfaces show higher interface energies and higher cohesion. In particular, the NW2 interface of Cu/W shows a relatively high W_{sep} in accordance with literature observations.

Overall, segregation towards the surfaces is stronger compared to segregation to the interfaces. Therefore, when present at the interface, the elements show a detrimental effect

on interface cohesion. The segregation energies calculated differ from previous calculations in W (Ti,Cl,S,Al,H,O) and Cu/W (H) in terms of absolute values, but the general trends are seen to be the same. Cl, a commonly known corroding element in both Cu and W, was used to determine the difference in segregation behavior of a W(Ti) bulk compared to a W bulk material. The main effect is that Cl is energetically stabilized by a Ti environment. However, the overall segregation trend remained the same as stabilization was comparable at the interface and the surface. A similar effect of other impurity atoms on W(Ti) is to be expected.

To counteract the effect of harmful impurities such as Cl, S, H, or O, either high purity materials are needed, or other elements with possible beneficial effects on cohesion need to be considered as well, e.g., B, C or Hf. Such co-segregation scenarios remain the object of future studies, for which the present work may serve as a methodological framework and showcase.

Author Contributions: Conceptualization, R.B. and L.R.; methodology, R.B., D.S. and L.R.; formal analysis, R.B., D.S., J.S. and L.R.; investigation, R.B. and L.R.; resources, J.S. and L.R.; writing—original draft preparation, R.B. and L.R.; writing—review and editing, R.B., D.S., J.S. and L.R.; visualization, R.B.; supervision, L.R.; project administration, J.S. and L.R.; funding acquisition, J.S. and L.R. All authors have read and agreed to the published version of the manuscript.

Funding: The authors gratefully acknowledge the financial support under the scope of the COMET program within the K2 Center "Integrated Computational Material, Process and Product Engineering (IC-MPPE)" (Project No. 886385). This program is supported by the Austrian Federal Ministries for Climate Action, Environment, Energy, Mobility, Innovation and Technology (BMK) and for Digital and Economic Affairs (BMDW), represented by the Austrian Research Promotion Agency (FFG), and the federal states of Styria, Upper Austria and Tyrol. This research was funded also in part by the Austrian Science Fund (FWF) (P 34179-N).

Data Availability Statement: Not applicable.

Conflicts of Interest: The authors declare no conflict of interest.

Appendix A. Remarks on Zr Segregation

The influence of Zr segregation on W_{sep} of the Cu/W interface reported by Wang et al. [38] is extremely high with an increase in cohesion by more than 300%. This is accompanied by a strongly negative γ that in turn would favor the spontaneous formation of a Cu-Zr/W pseudo alloy. As such, phenomena have not been reported in literature, and we take a closer look on this specific case for clarification.

Figure A1 compares the influence of Zr segregation on the W_{sep} of the Cu/W interface in a coherent cell with W lattice parameters calculated by Wang et al. [38] as well as in our semi-coherent cell. Our results show a much smaller effect, a strengthening of 0.1 J/m^2 of the W_{sep} on a Cu site and a weakening of -0.2 J/m^2 on a W site. A similar effect has been observed during our initial testing of segregation for different cell sizes and geometries. Cells with large strain or insufficient layer sizes would display a rearrangement of the Cu slab to accommodate the segregation element. This then affects γ as well as W_{sep} and the Cu slab of Cu-Zr/W would exhibit a different structure as the one in the Cu/W cell resulting in huge differences in energy. Our larger and strain optimized cell, however, shows no noticeable difference in relaxation in comparison to the cell without the segregation element.

Overall, this effect can be attributed to the strain on the system which was shown in our previous publication [43] to be 20 percent in one direction for a coherent Cu/W NW cell and 43 percent for a coherent KS cell. Such strains put the system under a huge pressure allowing the influence of a foreign agent such as the Zr atom to rearrange the Cu slab to another lower energy structure. However, it has to be noted that such a structure is not representative and a mere artefact of the assumed coherent interface structure. The pressure is noticeably lower in our semi-coherent Cu/W cell as the strain values after stress balancing are below 1 percent in both directions in our larger NW cell; therefore, a rearrangement of the Cu is not observed with the addition of Zr.

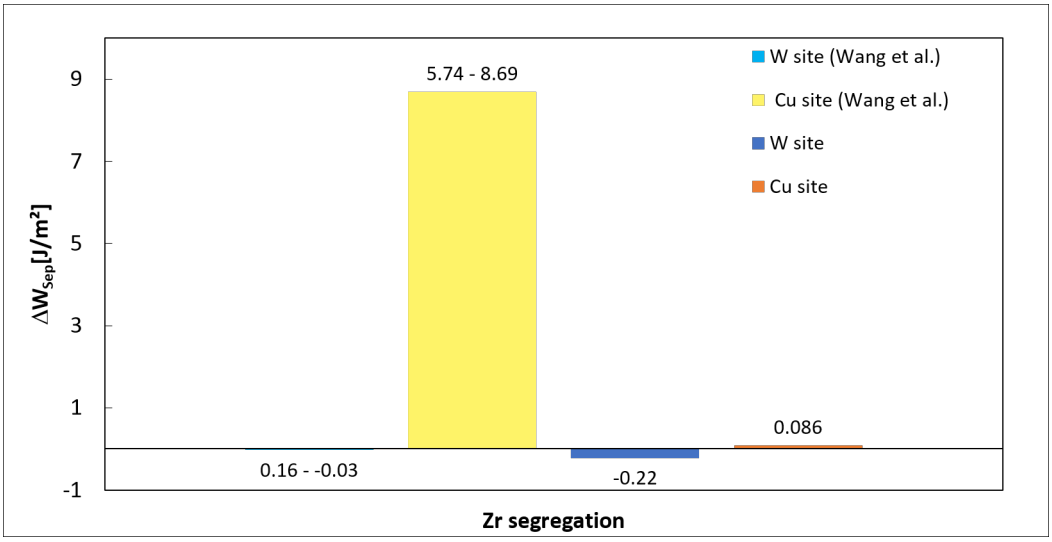


Figure A1. Comparison of Wang et al. [38] (**left**) and our results (**right**) on the influence of Zr on the W_{sep} of Cu/W.

References

1. Chen, P.; Shen, Q.; Luo, G.; Wang, C.; Li, M.; Zhang, L.; Li, X.; Zhu, B. Effect of interface modification by Cu-coated W powders on the microstructure evolution and properties improvement for Cu–W composites. *Surf. Coat. Technol.* **2016**, *288*, 8–14. [CrossRef]
2. Selvakumar, N.; Vettivel, S. Thermal, electrical and wear behavior of sintered Cu–W nanocomposite. *Mater. Des.* **2013**, *46*, 16–25. [CrossRef]
3. Hou, C.; Song, X.; Tang, F.; Li, Y.; Cao, L.; Wang, J.; Nie, Z. W–Cu composites with submicron- and nanostructures: Progress and challenges. *NPG Asia Mater.* **2019**, *11*, 74. [CrossRef]
4. Kong, Y.; Pi, J.; Xiao, S.; Du, Y. Asymmetric mixing behavior and stability of the predicted phases in the W-Cu system. *Calphad Comput. Coupling Phase Diagr. Thermochem.* **2016**, *53*, 116–121. [CrossRef]
5. Chen, Y.; Liu, B. Alloy phases formed in immiscible CuMo and CuW systems by multilayer-technique. *J. Alloys Compd.* **1997**, *261*, 217–224. [CrossRef]
6. Girault, B.; Eyidi, D.; Chauveau, T.; Babonneau, D.; Renault, P.O.; Le Bourhis, E.; Goudeau, P. Copper coverage effect on tungsten crystallites texture development in W/Cu nanocomposite thin films. *J. Appl. Phys.* **2011**, *109*, 014305. [CrossRef]
7. Ma, G.C.; Fan, J.L.; Gong, H.R. Fundamental effects of hydrogen on cohesion properties of Cu/W interfaces. *Solid State Commun.* **2017**, *250*, 79–83. [CrossRef]
8. Zong, R.L.; Wen, S.P.; Zeng, F.; Gao, Y.; Pan, F. Nanoindentation studies of Cu-W alloy films prepared by magnetron sputtering. *J. Alloys Compd.* **2008**, *464*, 544–549. [CrossRef]
9. Tarancón, S.; Tejado, E.; Richou, M.; Pastor, J. Evaluation of tensile and elastic properties of W/Cu cold-spray coatings for application to the FGM DEMO divertor concept. *Fusion Eng. Des.* **2021**, *171*, 112719. [CrossRef]
10. Moszner, F.; Cancellieri, C.; Chiodi, M.; Yoon, S.; Ariosa, D.; Janczak-Rusch, J.; Jeurgens, L. Thermal stability of Cu/W nano-multilayers. *Acta Mater.* **2016**, *107*, 345–353. [CrossRef]
11. Ruffini, A.; Durinck, J.; Colin, J.; Coupeau, C.; Grilhé, J. Gliding at interface during thin film buckling: A coupled atomistic/elastic approach. *Acta Mater.* **2012**, *60*, 1259–1267. [CrossRef]
12. Lloyd, J.R.; Clemens, J.; Snede, R. Copper metallization reliability. *Microelectron. Reliab.* **1999**, *39*, 1595–1602. [CrossRef]
13. Chiou, J.C.; Juang, K.C.; Chen, M.C. TiW(N) as Diffusion Barriers Between Cu and Si. *J. Electrochem. Soc.* **1995**, *142*, 2326–2331. [CrossRef]
14. Kleinbichler, A.; Todt, J.; Zechner, J.; Wöhlert, S.; Többens, D.; Cordill, M. Annealing effects on the film stress and adhesion of tungsten-titanium barrier layers. *Surf. Coat. Technol.* **2017**, *332*, 376–381.
15. Gao, Y.; Yang, T.; Xue, J.; Yan, S.; Zhou, S.; Wang, Y.; Kwok, D.T.; Chu, P.K.; Zhang, Y. Radiation tolerance of Cu/W multilayered nanocomposites. *J. Nucl. Mater.* **2011**, *413*, 11–15. [CrossRef]
16. Gładyszewski, G.; Pacaud, J.; Goudeau, P.; Jaouen, C.; Naudon, A.; Grilhé, J. Interface of the Cu multilayers. *Vacuum* **1994**, *45*, 285–287. [CrossRef]
17. Monclús, M.; Karlik, M.; Callisti, M.; Frutos, E.; LLorca, J.; Polcar, T.; Molina-Aldareguía, J. Microstructure and mechanical properties of physical vapor deposited Cu/W nanoscale multilayers: Influence of layer thickness and temperature. *Thin Solid Films* **2014**, *571*, 275–282.
18. Zheng, S.; Carpenter, J.S.; McCabe, R.J.; Beyerlein, I.J.; Mara, N.A. Engineering interface structures and thermal stabilities via SPD processing in bulk nanostructured metals. *Sci. Rep.* **2014**, *4*, 4226.
19. Kurdjumov, G.; Sachs, G. Over the mechanisms of steel hardening. *Z. Phys.* **1930**, *64*, 325–343.

20. Nishiyama, Z. X-ray investigation of the mechanism of the transformation from face centered cubic lattice to body centered cubic. *Sci. Rep. Tohoku Univ.* **1934**, *23*, 637.
21. Wang, J.; Zhang, R.F.; Zhou, C.Z.; Beyerlein, I.J.; Misra, A. Interface dislocation patterns and dislocation nucleation in face-centered-cubic and body-centered-cubic bicrystal interfaces. *Int. J. Plast.* **2014**, *53*, 40–55. [CrossRef]
22. Beyerlein, I.; Mara, N.; Carpenter, J.; Nizolek, T.; Mook, W.; Wynn, T.; McCabe, R.; Mayeur, J.; Kang, K.; Zheng, S.; et al. Interface-driven microstructure development and ultra high strength of bulk nanostructured Cu-Nb multilayers fabricated by severe plastic deformation. *J. Mater. Res.* **2013**, *28*, 1799–1812. [CrossRef]
23. Wang, J.; Kang, K.; Zhang, R.; Zheng, S.; Beyerlein, I.; Mara, N. Structure and Property of Interfaces in ARB Cu/Nb Laminated Composites. *JOM* **2012**, *64*, 1208–1217. [CrossRef]
24. Lejček, P.; Šob, M. An analysis of segregation-induced changes in grain boundary cohesion in bcc iron. *J. Mater. Sci.* **2014**, *49*, 2477–2482. [CrossRef]
25. Lejcek, P. *Grain Boundary Segregation in Metals*; Springer Series in Materials Science; Springer: Berlin/Heidelberg, Germany, 2010.
26. Divinski, S.V.; Edelhoff, H.; Prokofjev, S. Diffusion and segregation of silver in copper $\Sigma5(310)$ grain boundary. *Phys. Rev. B* **2012**, *85*, 144104. [CrossRef]
27. Hirsimäki, M.; Lampimäki, M.; Lahtonen, K.; Chorkendorff, I.; Valden, M. Investigation of the role of oxygen induced segregation of Cu during Cu_2O formation on Cu100, Ag/Cu100 and Cu(Ag) alloy. *Surf. Sci.* **2005**, *583*, 157–165. [CrossRef]
28. Surholt, T.; Mishin, Y.M.; Herzig, C. Grain-boundary diffusion and segregation of gold in copper: Investigation in the type-B and type-C kinetic regimes. *Phys. Rev. B* **1994**, *50*, 3577–3587. [CrossRef]
29. Scheiber, D.; Pippan, R.; Puschnig, P.; Romaner, L. Ab initio calculations of grain boundaries in bcc metals. *Model. Simul. Mater. Sci. Eng.* **2016**, *24*, 035013. [CrossRef]
30. Zhang, B.; Li, Y.H.; Zhou, H.B.; Deng, H.; Lu, G.H. Segregation and aggregation of rhenium in tungsten grain boundary: Energetics, configurations and strengthening effects. *J. Nucl. Mater.* **2020**, *528*, 151867. [CrossRef]
31. Zhou, H.B.; Jin, S.; Zhang, Y.; Lu, G.H. Effects of hydrogen on a tungsten grain boundary: A first-principles computational tensile test. *Prog. Nat. Sci. Mater. Int.* **2011**, *21*, 240–245. [CrossRef]
32. Setyawan, W.; Kurtz, R.J. Ab initio study of H, He, Li and Be impurity effect in tungsten $\Sigma3112$ and $\Sigma27552$ grain boundaries. *J. Phys. Condens. Matter* **2014**, *26*, 135004. [CrossRef]
33. He, W.; Gao, X.; Zhou, L.; Yang, D.; Wang, Z. First-principles investigation of grain boundary structure effects on hydrogen solubility and segregation in tungsten. *J. Nucl. Sci. Technol.* **2021**, *58*, 207–217. [CrossRef]
34. Gludovatz, B.; Wurster, S.; Weingärtner, T.; Hoffmann, A.; Pippan, R. Influence of impurities on the fracture behaviour of tungsten. *Philos. Mag.* **2011**, *91*, 3006–3020. [CrossRef]
35. Razumovskiy, V.I.; Divinski, S.V.; Romaner, L. Solute segregation in Cu: DFT vs. Experiment. *Acta Mater.* **2018**, *147*, 122–132. [CrossRef]
36. Hono, K.; Pickering, H.; Hashizume, T.; Kamiya, I.; Sakurai, T. Oxygen segregation and oxidation on a copper surface. *Surf. Sci.* **1989**, *213*, 90–102. [CrossRef]
37. Nieh, T.G.; Nix, W.D. Embrittlement of copper due to segregation of oxygen to grain boundaries. *Metall. Trans. A* **1981**, *12*, 893–901. [CrossRef]
38. Wang, J.W.; Fan, J.L.; Gong, H.R. Effects of Zr alloying on cohesion properties of Cu/W interfaces. *J. Alloys Compd.* **2016**, *661*, 553–556. [CrossRef]
39. González, C.; Iglesias, R. Energetic analysis of He and monovacancies in Cu/W metallic interfaces. *Mater. Des.* **2016**, *91*, 171–179. [CrossRef]
40. Chookajorn, T.; Schuh, C.A. Nanoscale segregation behavior and high-temperature stability of nanocrystalline W-20 at.% Ti. *Acta Mater.* **2014**, *73*, 128–138. [CrossRef]
41. Ångqvist, M.; Rahm, J.M.; Gharaee, L.; Erhart, P. Structurally driven asymmetric miscibility in the phase diagram of W-Ti. *Phys. Rev. Mater.* **2019**, *3*, 073605. [CrossRef]
42. Bodlos, R.; Dengg, T.; Ruban, A.V.; Dehghani, M.; Romaner, L.; Spitaler, J. Ab initio investigation of the atomic volume, thermal expansion, and formation energy of WTi solid solutions. *Phys. Rev. Mater.* **2021**, *5*, 043601. [CrossRef]
43. Bodlos, R.; Fotopoulos, V.; Spitaler, J.; Shluger, A.; Romaner, L. Energies and structures of Cu/Nb and Cu/W interfaces from density functional theory and semi-empirical calculations. *Materialia* **2022**, *21*, 101362. [CrossRef]
44. Cowley, J.M. An Approximate Theory of Order in Alloys. *Phys. Rev.* **1950**, *77*, 669–675. [CrossRef]
45. Cowley, J.M. Short-Range Order and Long-Range Order Parameters. *Phys. Rev.* **1965**, *138*, A1384–A1389. [CrossRef]
46. Warren, B. *X-ray Diffraction*; Dover Publication: New York, NY, USA, 1990; p. 381.
47. Perdew, J.P.; Chevary, J.A.; Vosko, S.H.; Jackson, K.A.; Pederson, M.R.; Singh, D.J.; Fiolhais, C. Atoms, molecules, solids, and surfaces: Applications of the generalized gradient approximation for exchange and correlation. *Phys. Rev. B* **1992**, *46*, 6671.
48. Popov, M.N.; Spitaler, J.; Mühlbacher, M.; Walter, C.; Keckes, J.; Mitterer, C.; Draxl, C. $TiO_2(100)/Al_2O_3(0001)$ interface: A first-principles study supported by experiment. *Phys. Rev. B* **2012**, *86*, 205309.
49. Demkowicz, M.; Hoagland, R. Structure of Kurdjumov–Sachs interfaces in simulations of a copper–niobium bilayer. *J. Nucl. Mater.* **2008**, *372*, 45–52. [CrossRef]
50. An, Q.; Yang, W.; Liu, B.; Zheng, S. Interface effects on the properties of Cu–Nb nanolayered composites. *J. Mater. Res.* **2020**, *35*, 2684–2700. [CrossRef]

51. Beyerlein, I.; Mara, N.; Wang, J.; Carpenter, J.; Zheng, S.; Han, W.; Zhang, R.; Kang, K.; Nizolek, T.; Pollock, T. Structure–property–functionality of bimetal interfaces. *JOM* **2012**, *64*, 1192–1207.
52. Liang, C.P.; Fan, J.L.; Gong, H.R.; Liao, X.; Zhu, X.; Peng, S. Interface structure and work function of W-Cu interfaces. *Appl. Phys. Lett.* **2013**, *103*, 211604.
53. Wang, A.Y.; Chen, B.; Fang, L.; Yu, J.J.; Wang, L.m. Influence of branched quaternary ammonium surfactant molecules as levelers for copper electroplating from acidic sulfate bath. *Electrochim. Acta* **2013**, *108*, 698–706. [CrossRef]
54. Alfreider, M.; Bodlos, R.; Romaner, L.; Kiener, D. The influence of chemistry on the interface toughness in a WTi-Cu system. *Acta Mater.* **2022**, *230*, 117813. [CrossRef]

Disclaimer/Publisher's Note: The statements, opinions and data contained in all publications are solely those of the individual author(s) and contributor(s) and not of MDPI and/or the editor(s). MDPI and/or the editor(s) disclaim responsibility for any injury to people or property resulting from any ideas, methods, instructions or products referred to in the content.